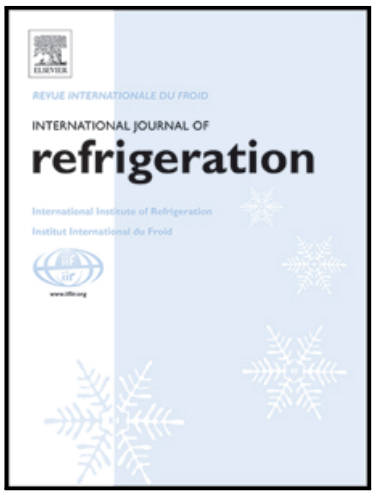

Simplified performance correlation of an indirect evaporative cooling system: development and validation

Francisco Comino , Samanta Milani , Stefano De Antonellis , Cesare Maria Joppolo , Manuel Ruiz de Adana

PII: S0140-7007(18)30033-1
DOI: 10.1016/j.ijrefrig.2018.02.002
Reference: JIJR 3876

To appear in: *International Journal of Refrigeration*

Received date: 4 September 2017
Revised date: 23 February 2018
Accepted date: 25 February 2018

Please cite this article as: Francisco Comino , Samanta Milani , Stefano De Antonellis , Cesare Maria Joppolo , Manuel Ruiz de Adana , Simplified performance correlation of an indirect evaporative cooling system: development and validation, *International Journal of Refrigeration* (2018), doi: 10.1016/j.ijrefrig.2018.02.002

Highlights

- An empirical simplified model of an indirect evaporative cooler is proposed.
- The model obtained was compared with a detailed model and with experimental data.
- The simplified model presents good accuracy and low computational load.

Title

Simplified performance correlation of an indirect evaporative cooling system: development and validation

Authors

Francisco Comino [a *], Samanta Milani[b], Stefano De Antonellis[b], Cesare Maria Joppolo[b], Manuel Ruiz de Adana[a]

[*] Corresponding author tel. +34 626285994; e-mail: francisco.comino@uco.es

Affiliations

[a] Departamento de Química-Física y Termodinámica Aplicada, Escuela Politécnica Superior, Universidad de Córdoba, Campus de Rabanales, Antigua Carretera Nacional IV, km 396, 14071 Córdoba, Spain

[b] Dipartimento di Energia, Politecnico di Milano, Via Lambruschini, 4, 20156 Milan, Italy

Abstract

At present, there is an increasing interest in indirect evaporative coolers (IEC), which are an effective alternative to conventional cooling systems due to their high efficiency. In this study a new simplified first order linear regression model of an IEC system has been developed. The model is based on experimental data and results of the proposed correlation have been compared with ones of a phenomenological model and with further measurements collected in significant operating conditions (data center, desiccant evaporative cooling cycle and residential application). It is shown that deviations of wet bulb effectiveness are limited to 3.4% for the simplified model and 2.1% for the detailed one. Therefore, due to its good accuracy and low computational load, the simplified model could be suitable to be implemented in simulation tools.

Keywords:

Indirect evaporative cooling, experimental, numerical, model

Nomenclature

$A_{HE,net}$	net heat exchanger cross area [m^2]
b_1-b_{15}	correlation parameters of the simplified model
cp	specific heat [J kg^{-1} K^{-1}]
c_1-c_4	correlation parameters of the detailed model
C_W	wettability coefficient [-]
h	net channel height [m]
H_{HE}	heat exchanger height [m]
h_M	convective mass transfer coefficient [kg s^{-1} m^{-2}]
h_T	convective heat transfer coefficient [W m^{-2} K^{-1}]
k	thermal conductivity [W m^{-1} K^{-1}]
k_1-k_4	correlation parameters of the detailed model
L*	net plate length and width [m]
$\dot{m}$	specific mass flow rate [kg s^{-1} m^{-2}]
$\dot{M}$	mass flow rate [kg s^{-1}]
N_T	number of tests [-]
N_0-N_{43}	reference test
N_{HE}	number of heat exchanger plate [-]
p	pressure [Pa]
pt	plates pitch [m]
RH	relative humidity [%]
$\dot{Q}$	air volumetric flow rate [m^3 h^{-1}]
$\dot{Q}_w$	water volumetric flow rate [l h^{-1}]
T	dry bulb temperature [°C]
t_{95}	student's multiplier at the 95% confidence level
T_{wb}	wet bulb temperature [ºC]
$u_{xi,inst}$	instrument uncertainty
u_{xi}	experimental uncertainty of quantity x_i
u_y	generic combined uncertainty
U_T	overall heat transfer coefficient [W m^{-2} K^{-1}]
v	air velocity [m s^{-1}]
V	simplified model input
x	primary air flow direction [m]

x_i	generic monitored variable
X	humidity ratio [$g_v\ kg_{da}^{-1}$]
y	secondary air flow direction [m]
y_i	generic calculated quantity
Y	generic system output

Greek letters

Δ	variation
δ	plate thickness [m]
δ_w	water film thickness [m]
ε_{db}	dry bulb effectiveness [-]
ε_h	saturation efficiency [-]
ε_{wb}	wet bulb effectiveness [-]
ρ	density [kg m^{-3}]
σ	wettability factor [-]
$\sigma_{\bar{x}_i}$	standard deviation of the mean

Superscripts

N	reference density (ρ=1.2 kg m^{-3})
EXP	experimental
NUM	numerical
'	referred to modified IEC systems (different number of plates)

Subscripts

a	air
HE	heat exchanger
in	inlet
min	minimum
out	outlet
p	primary air
s	secondary air
v	water vapour
w	liquid water

Acronyms

DM	detailed model
DOE	design of experiments
IEC	indirect evaporative cooler or cooling
MD	maximum deviation
RMSD	root mean standard deviation
SM	simplified model

1. Introduction

Indirect evaporative cooling (IEC) systems are an effective alternative to conventional technologies, due to their high efficiency and reduced primary energy consumption (Duan et al., 2012). In an IEC system, the primary air stream is cooled at constant humidity ratio in a heat exchanger, which is crossed by a secondary air stream humidified with liquid water.

The IEC technology can be used in many applications: in pre-cooling and energy recovery units (Chen et al., 2014; Cui et al., 2015), in two stage indirect/direct evaporative cooling systems (Elgendy et al., 2015; Heidarinejad et al., 2009), in passive cooling units (González Cruz and Krüger, 2015) or in combination with desiccant dehumidifiers (Chung and Lee, 2011; Goldsworthy and White, 2011; Pandelidis et al., 2016). Furthermore, recent studies highlight that the use of IEC systems in data centres leads to significant energy savings (Agrawal et al., 2016).

Many research studies available in literature deal with IEC systems, in particular focusing on the optimization of the device and on the effect of operating parameters on outlet air conditions. The performance of IEC systems has been analysed in detail, evaluating the effect of variable inlet air velocities (Velasco Gómez et al., 2012), different constructive parameters, such as material and geometry (Gómez et al., 2005; Tejero-González et al., 2013), or variable water flow rate (De Antonellis et al., 2016).

Mathematical models of IECs are very useful to optimize the device as well as to study the behaviour of the system when it is combined with other HVAC components. Maclaine-cross and Banks (1981) developed an analytical model using a linearized approximate theory for a thin and continuous water layer inside the wet channels. Erens and Dreyer (1993) presented a simplified finite volume model, based on the models of Poppe and Rögener (1984) and Merkel (1925) for the analysis of direct contact cooling towers. Kim et al. (2011) studied a finite difference method using an equivalent temperature at the interface. Ren and Yang (2006) elaborated a detailed mathematical model, considering the heat and mass transfer in the IEC with parallel or counter flow configurations and taking into account partial surface wetting conditions and water temperature variation. Hasan (2012) developed a model to analyse the

thermal performance through a *ε-NTU* approach. Guo and Zhao (1998) carried out a numerical analysis to investigate the heat and mass transfer phenomena occurring in a cross flow IEC, evaluating the effect of plates wettability and the variation of inlet air velocity. Hettiarachchi et al. (2007) developed a finite difference method based on the NTU approach to investigate the effect of longitudinal heat conduction. Cui et al. (2014) developed a computational model to study the effect of main parameters on a counter-flow dew point evaporative cooler. De Antonellis et al. (2017) proposed a mathematical model of a IEC system, taking into account the effect of adiabatic humidification of the secondary air stream and the wettability factor of the heat exchanger surface. However, most of the aforementioned approaches, due to the high computational load, cannot be easily implemented in energy simulation tools.

Another mathematical modelling approach recently used to obtain simplified models of IEC systems is based on statistical design (Montgomery, 2004). A simplified model generated by response surface methodology was presented for analysing performance of a device based on the M-cycle (Pandelidis and Anisimov, 2016). Other authors obtained a mathematical model to determine the performance of a M-cycle crossflow heat exchanger, based on a statistical method known as "group method of data handling-type neural network" (Sohani et al., 2016). Both statistical models accurately represented the behaviour of an IEC M-cycle system and they could be easily integrated into HVAC models.

Finally, the aim of this work is to develop a simplified IEC model based on experimental data, which can be easily introduced in HVAC system simulation tools. Obtained results are compared with outputs of a previously developed phenomenological model (De Antonellis et al., 2017) and with further laboratory tests of the device. In particular, the proposed simplified model includes the effect of variable water flow rate, which has a significant effect on system performance.

2. Experimental set up

2.1 Description of the evaluated IEC system

The analysed indirect evaporative cooling system is composed of the following elements:

- A commercial crossflow plate heat exchanger.
- 8 water nozzles installed in the secondary airflow inlet plenum.
- A water pumping system.

As shown in Fig. 1, two air streams cross the heat exchanger:

- The primary air stream, which enters the system in condition *p,in* and leaves the component in condition *p,out*. This air stream is cooled at constant humidity ratio.
- The secondary air stream, which enters and leaves the system respectively in condition *s,in* and *s,out*. It is supplied to the upper part of the system, where spray nozzles are installed, flowing from the top to the bottom of the device. First, due to the evaporation of water droplets in the inlet plenum, the secondary air stream is humidified almost at constant enthalpy and it reaches the heat exchanger face in condition *s,in,HE*. Then, the secondary air stream passes through the heat exchanger plates, where a further water evaporation occurs.

The net face heat exchanger cross area $A_{net,HE}$ (equal to 0.089 m^2) and height H_{HE} are evaluated respectively with Eq. 1 and Eq. 2:

$$A_{net,HE}=(H_{HE} - N_{HE}\cdot\delta)\cdot L^* / 2 \quad (1)$$

$$H_{HE}= (N_{HE}-1)\ pt + \delta \quad (2)$$

Plates are made of aluminium alloy with semi spherical dimples. The water nozzles are installed on two parallel manifolds, which are 15 cm far from the heat exchanger face. Eight axial and full cone type nozzles are used, as shown in Fig. 1 (two stoppers are mounted in the middle of the system). The nominal water flow rate of each one is 7.50 l h^{-1} at 9 bar. The water is supplied in counter current arrangement respect to the secondary air stream through a commercial pumping unit, without any recirculation to minimize the risk of contamination. Finally, the length of top and side plenums is 42 cm.

Table 1. Main characteristics of the heat exchanger.

Description	Parameter	Value
Plates material	-	Aluminium alloy
Number of plates	N_{HE}	119
Plate thickness	δ	0.14 mm
Plate pitch	pt	3.35 mm
Net channel height	$h=pt-\delta$	3.21 mm
Net plate length and width	L^*	470 mm
Net face heat exchanger cross area	$A_{HE,net}$	0.089 m^2

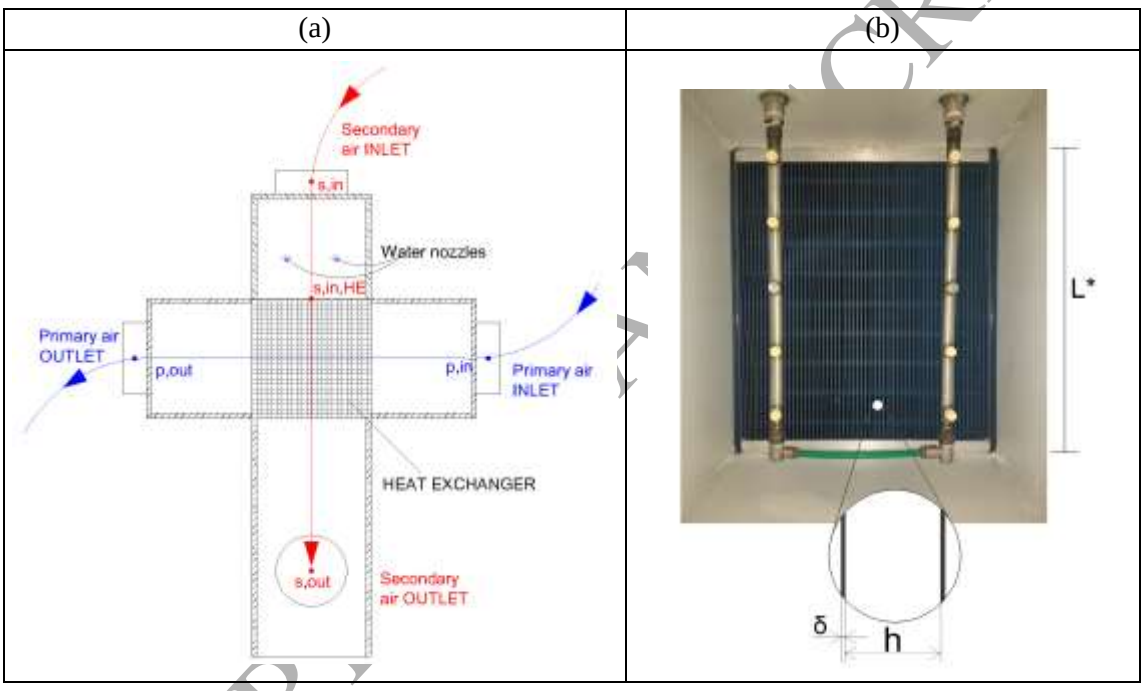

Fig. 1. (a) Scheme of the investigated indirect evaporative cooling system and (b) picture of the secondary air inlet plenum.

2.2 Description of the test rig and experimental methodology

The primary and secondary airflow conditions are controlled by two independent air handling units. Temperature and humidity ratio of each stream are set through heating and cooling coils, evaporative humidifiers and electric heaters. The maximum volumetric flow rates of the primary and secondary air streams are respectively 1400 m^3 h^{-1} and 2000 m^3 h^{-1}. Each air flow rate is measured using two orifice plates and piezo resistive pressure transmitters placed in two different measurement ducts, constructed according to standards (DIN EN ISO 5167-2 Standards, 2003). The two air handling units can work in outdoor or recirculated air mode, depending on the desired supply air conditions.

The water flow rate supplied to the nozzles from the pumping unit was measured using a turbine flow sensor, whose accuracy is 3% of the reading. A detailed test rig description has been reported in a previous work of the authors (De Antonellis et al., 2016), while adopted instruments data are shown in Table 2.

Table 2. Technical specification of measuring devices.

Physical quantity	Type of sensor	Accuracy[a]
T^b	PT 100 Class A	±0.2 °C
RH^b	Capacitive	±1% (between 0 and 90%)
p	Piezo resistive	0.5% of reading ±1 Pa

[a] at T=20 °C
[b] Temperature and relative humidity probe

In each experimental session, at least 300 samples of each physical quantity have been collected in steady state conditions and at a frequency of 1 Hz. The experimental uncertainty u_{xi} of each direct monitored variable x_i (T, RH, p) is:

$$u_{x_i} = \pm\sqrt{u_{x_{i,inst}}^2 + (t_{95}\,\sigma_{\overline{x_i}})^2} \tag{3}$$

Where $u_{xi,inst}$ is the instrument uncertainty of the measured quantity t_{95} is the Student test multiplier al 95% confidence and $\sigma_{\overline{x_i}}$ is the standard deviation of the mean.

The generic combined uncertainty u_y of calculated quantities y_i, such as ε_{wb}, ΔT_p, ΔT_s and ΔX_s is calculated as:

$$u_{y_i} = \sqrt{\sum_i \left(\frac{\partial y_i}{\partial x_i} u_{x_i,inst}\right)^2 + t_{95}^2 \sum_i \left(\frac{\partial y_i}{\partial x_i}\sigma_{\overline{x_i}}\right)^2} \tag{4}$$

The uncertainty of the evaluated quantities are estimated in accordance with Moffat (1988). The methodology and the assumptions are described in the reference international standard (ISO, 2008).

2.3 Performance indexes and preliminary experimental results

Experimental results have been evaluated in terms of wet bulb effectiveness ε_{wb}, of variation of primary air temperature ΔT_p, secondary air temperature ΔT_s, and secondary air humidity ratio ΔX_s. Such indexes are defined through the following equations:

$$\varepsilon_{wb} = \frac{\left(T_{p,in} - T_{p,out}\right)}{\left(T_{p,in} - T_{wb,s,in}\right)} \tag{5}$$

$$\Delta T_p = T_{p,in} - T_{p,out} \tag{6}$$

$$\Delta T_s = T_{s,in} - T_{s,out} \quad (7)$$

$$\Delta X_s = X_{s,out} - X_{s,in} \quad (8)$$

According to Table 3, 82 tests of the IEC system have been performed for the calibration and validation of both models. More precisely, 30 tests have been used to calibrate the detailed model (De Antonellis et al., 2017; Liberati et al., 2017) and 37 tests to develop the linear regression correlation. Finally, 15 tests have been carried out to validate and compare results of both models. As discussed in detail in section 4.2, operating conditions of these tests have been selected in order to reproduce significant application of IEC system: data center, desiccant evaporative cycle and residential application.

Table 3. Summary of test conditions for calibration and validation of the models.

$N_{1\text{-}26}$ [a]	Model	N_T	$T_{s,in}$ [°C]	$X_{s,in}$ [g_v kg_{da}^{-1}]	v_s^N [m s^{-1}]	$T_{p,in}$ [b] [°C]	$\dot{Q}_{w,in}$ [l h^{-1}]
N_1	DM	5	30.0	10.6	3.7	35.0	30, 35, 45, 55, 65
N_2	DM	5	30.0	10.6	5.7	35.0	30, 35, 45, 55, 65
N_3	DM	5	30.0	13.4	3.7	35.0	30, 35, 45, 55, 65
N_4	DM	5	30.0	13.4	5.7	35.0	30, 35, 45, 55, 65
N_5	DM	5	36.8	10.6	3.7	35.0	30, 35, 45, 55, 65
N_6	DM	5	36.8	10.6	5.7	35.0	30, 35, 45, 55, 65
N_7	SM	2	25.0	8.0	3.7	28.0	30, 60
N_8	SM	2	25.0	8.0	5.7	28.0	30, 60
N_9	SM	2	25.0	8.0	3.7	48.0	30, 60
N_{10}	SM	2	25.0	8.0	5.7	48.0	30, 60
N_{11}	SM	2	25.0	16.0	3.7	28.0	30, 60
N_{12}	SM	2	25.0	16.0	5.7	28.0	30, 60
N_{13}	SM	2	25.0	16.0	3.7	48.0	30, 60
N_{14}	SM	2	25.0	16.0	5.7	48.0	30, 60
N_{15}	SM	2	38.0	8.0	3.7	28.0	30, 60
N_{16}	SM	2	38.0	8.0	5.7	28.0	30, 60
N_{17}	SM	2	38.0	8.0	3.7	28.0	30, 60
N_{18}	SM	2	38.0	8.0	5.7	28.0	30, 60
N_{19}	SM	2	38.0	16.0	3.7	28.0	30, 60
N_{20}	SM	2	38.0	16.0	5.7	28.0	30, 60
N_{21}	SM	2	38.0	16.0	3.7	28.0	30, 60
N_{22}	SM	2	38.0	16.0	5.7	28.0	30, 60
N_{23}	SM	5	31.5	12.0	4.7	38.0	45
N_{24}	DM, SM	5	30.0	13.3	4.7	35.0	30, 35, 45, 55, 65
N_{25}	DM, SM	5	26.0	12.6	3.7	60.0	30, 35, 45, 55, 65
N_{26}	DM, SM	5	26.0	12.6	3.7	30.0	30, 35, 45, 55, 65

[a] Tests N_1 - N_{23} for calibration of the models, Tests N_{24} - N_{26} for validation of the models

[b] v_p^N=3.7 m s^{-1} and $X_{p,in}$ =10.0 g_v kg_{da}^{-1}.

In Table 3 the air velocity is referred to reference air density (ρ_a^N=1.2 kg m^{-3}) and calculated through Eq. 9, where $\dot{Q}_a^N$ is the volumetric airflow rate.

$$v_a^N = \dot{Q}_a^N / (3600 \cdot A_{HE,net}) \quad (9)$$

For instance, when v^N_a= 3.7 m s^{-1}, the volumetric airflow rate is around 1200 m^3 h^{-1}.

The measured dry bulb effectiveness of the crossflow heat exchanger is 62.1 % (at v_s^N= v_p^N= 3.7 m s^{-1}, $T_{p,in}$= 31°C and $T_{s,in}$= 50°C), which is calculated by Eq. 10. The nominal pressure drop across the heat exchanger is 100 Pa when v_a = 3.2 m s^{-1} (at T_a= 35°C).

$$\varepsilon_{db}=\dot{M}_p \cdot cp_p \cdot (T_{p,in} - T_{p,out}) / [(\dot{M}_a \cdot cp_a)_{\min} (T_{p,in} - T_{s,in})] \quad (10)$$

In Fig. 2 typical trends of adopted performance indexes are reported (tests N_1 and N_2 of Table 3). In the investigated conditions, the maximum wet bulb effectiveness is equal to 86% and the maximum primary air temperature difference is close to 13 °C. A detailed analysis of trends of the IEC performance indexes has been provided in a previous research of the authors (De Antonellis et al., 2016). It is highlighted that in the present work, due to a different setup, IEC system performs slightly better: ε_{wb} values, at the same operating conditions, are 1-2% higher than those obtained in the previous research. In this study, wider air plenums have been adopted, enhancing adiabatic humidification of the secondary air stream and promoting a uniform water distribution on the heat exchanger face. The difference deals only with air plenums, while the heat exchanger and the humidification system are the same.

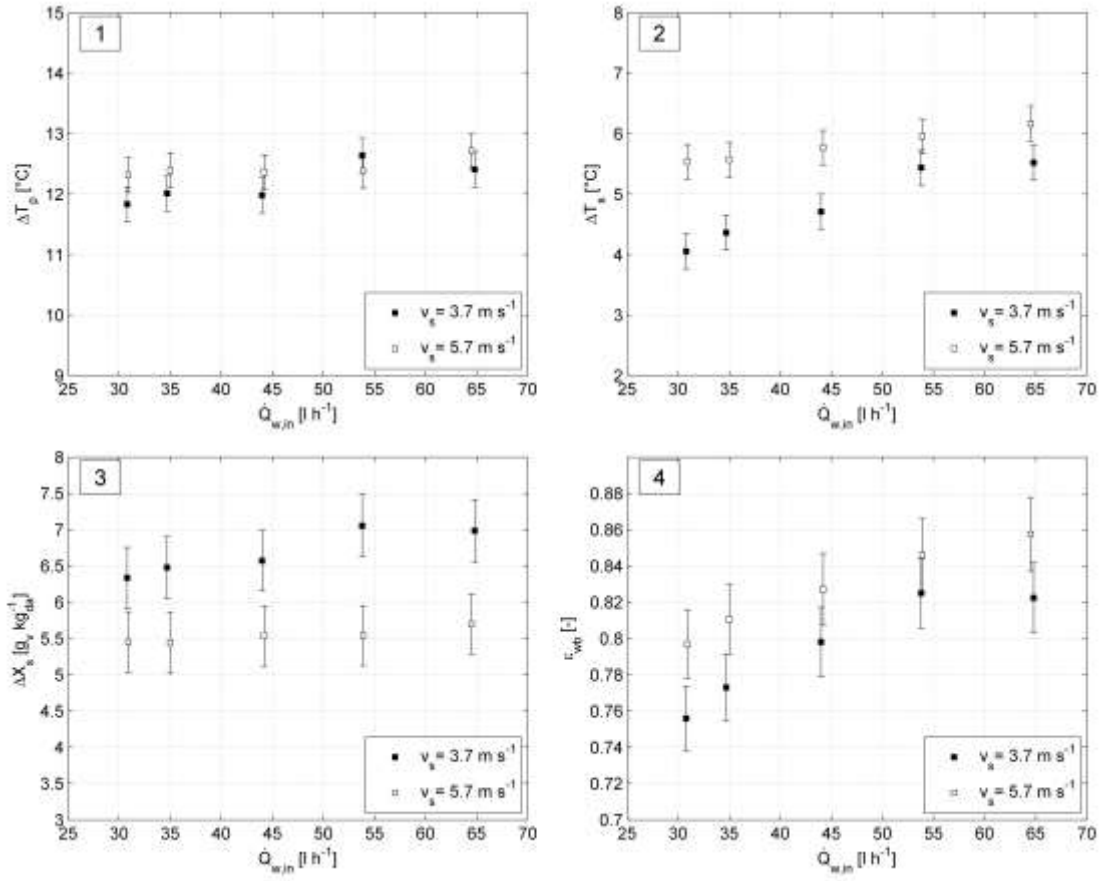

Fig. 2. Experimental data of the investigated IEC system in test N_1 (v_s^N=3.7 m s^{-1}) and N_2 (v_s^N=5.7 m s^{-1}) reported in Table 3.

3. Models description

3.1 Adopted approach

In this work, two indirect evaporative cooling models are discussed: a simplified model (SM), based on a first order linear regression approach and a detailed model (DM), based on heat and mass transfer equations. As described in detail in sections 3.2 and 3.3, both IEC models have been properly calibrated through specific set of experimental data, summarized in Table 3 and denoted with acronyms SM and DM. Finally, the numerical results obtained with the two models have been analysed and compared with a further set of experimental data, representative of possible operating conditions of the IEC system.

3.2 Simplified model (SM)

A new empirical simplified model has been developed in this work to predict the behaviour of the air outlet conditions of the IEC system. The methodology used to fit this model is based on the statistical technique of design of experiments, DOE, (Montgomery, 2004). The fit of the model and its further statistical analysis have been carried out through a commercial software (Statgraphics Centurion XV, 2006).

In this work, a DOE with three output variables and five input variables, namely $T_{p,in}$, $T_{s,in}$, $X_{s,in}$, v_s^N and $\dot{Q}_{w,in}$ has been developed. The input variables range has been defined in order to have representative operating conditions of actual IEC systems. The primary air velocity has been set constant and equal to typical working conditions, reducing the required number of experimental tests. The output process variables are the outlet primary air temperature, $T_{p,out}$, the outlet secondary air temperature, $T_{s,out}$, and the outlet secondary air humidity ratio, $X_{s,out}$. The effect of the five input variables is studied using the factorial design approach, design at 2-levels (Montgomery, 2004). The factorial design method is frequently applied to experimental works when the response is approximately linear within the selected input variables range. The total number of required experimental tests (N_T) to carry out the factorial design is defined by Eq. 11, where n is the number of input variables and R_c is the replicate number of an interior point (Montgomery, 2004):

$$N_T = 2^n + R_c \tag{11}$$

In this work, in order to evaluate the repeatability of the measurement system and estimate whether there are nonlinear processes, 5 replicates of the central point are included (N_{23}), leading to a set of 37 experimental tests, summarized in Table 3 (N_7 - N_{23}).

The relationship between the output and input variables was examined using first order polynomial equations. The resulting polynomial equation model is expressed by Eq. 12, where

Y^{NUM} is the predicted output value, V_i is a term equal to each input variable or, in case of correlation, to the product of two input variables and $b_i/1000$ are the regression coefficients.

$$Y^{NUM} = \frac{b_0 + \sum_{i=1}^{15} b_i V_i}{1000} \quad (12)$$

The estimated coefficients $b_{0\text{-}15}$ and the terms $V_{1\text{-}15}$ of Eq. 12 are summarized in Table 4. It can be observed that the coefficients with the highest weight are b_3 for $T_{p,out}$ and b_4 for $T_{s,out}$ and $X_{s,out}$.

The accuracy of the model to predict the experimental outlet conditions is reported in terms of R^2 values. More precisely, R^2 values, obtained considering all the 37 tests, are 99.54 % for $T_{p,out}$, 99.78 % for $T_{s,out}$ and 99.89 % for $X_{s,out}$.

Table 4. Estimated coefficients of the simplified model (SM) of Eq. 12.

Estimated coefficients	V_i	$T_{p,out}$ [ºC]	$T_{s,out}$ [ºC]	$X_{s,out}$ [g_v kg_{da}^{-1}]
b_0	-	-1313.76	3801.74	-379.62
b_1	$T_{p,in}$	322.41	500.49	183.23
b_2	$T_{s,in}$	364.07	191.57	135.71
b_3	$X_{s,in}$	766.52	455.43	313.29
b_4	v_s^N	-467.09	-1199.63	755.41
b_5	$\dot{Q}_{w,in}$	41.87	20.99	3.33
b_6	$T_{p,in} \cdot T_{s,in}$	0.42	0.60	0.19
b_7	$T_{p,in} \cdot X_{s,in}$	-5.09	-3.93	6.28
b_8	$T_{p,in} \cdot v_s^N$	-15.66	-25.34	-35.06
b_9	$T_{p,in} \cdot \dot{Q}_{w,in}$	-1.23	-2.02	1.12
b_{10}	$T_{s,in} \cdot X_{s,in}$	-8.45	-5.85	3.32
b_{11}	$T_{s,in} \cdot v_s^N$	26.11	42.55	-6.63
b_{12}	$T_{s,in} \dot{Q}_{w,in}$	-2.11	-1.54	0.92
b_{13}	$X_{s,in} \cdot v_s^N$	12.58	19.45	33.91
b_{14}	$X_{s,in} \dot{Q}_{w,in}$	2.87	3.37	-2.39
b_{15}	$v_s^N \dot{Q}_{w,in}$	-0.94	3.94	-4.54

Finally, in Fig. 3 it is shown that difference between numerical and experimental ΔT_p is always within 0.5 °C.

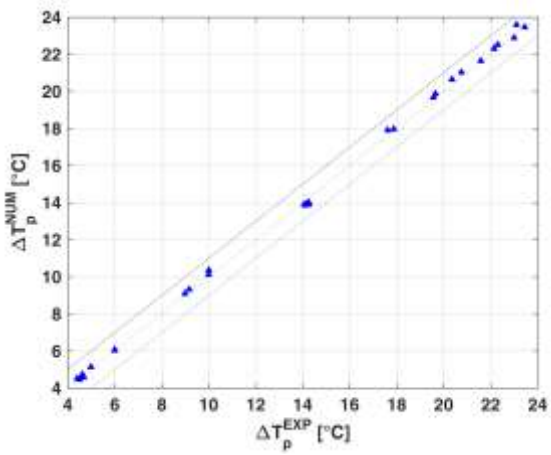

Fig. 3. Parity plot of experimental and numerical ΔT_p of the simplified model (tests N_7 - N_{23} reported in Table 3).

3.3 Detailed model (DM)

The detailed model (DM) is based on the solution of heat and mass transfer equations in the crossflow heat exchanger. It takes into account also the water droplets evaporation in the secondary inlet air plenum and the fraction of wet surface of heat exchanger plates. Assumptions, governing equations and calibration procedure of the model have been discussed in detail in a previous work of the authors (De Antonellis et al., 2017). Therefore, in this research only a brief description of the model is reported.

Main adopted assumptions are: i) Steady-state conditions; ii) No heat losses to the surroundings; iii) Negligible axial heat conduction and water diffusion in the air streams; iv) Negligible heat conduction along heat exchanger plates; v) Uniform air inlet conditions; vi) Interface plate temperature equal to bulk water temperature.

Governing equations applied to the primary air stream, to the secondary air stream and to the heat exchanger surface and water layer are:

$$\frac{dT_p}{dx} = \frac{U_{T,p}\left(T_W - T_p\right)}{v_p cp_p \rho_p \frac{h}{2}} \tag{13}$$

$$\frac{dT_s}{dy} = \frac{h_{T,s}\left(T_W - T_s\right)}{v_s cp_s \rho_s \frac{h}{2}} + \frac{h_{M,s}\left(\lambda + cp_s T_s\right)\left(X_W - X_s\right)\sigma}{v_s cp_s \rho_s \frac{h}{2}} \tag{14}$$

$$\frac{dX_s}{dy} = \frac{h_{M,s}\left(X_W - X_s\right)\sigma}{v_s \rho_s \frac{h}{2}} \tag{15}$$

$$h_{M,s}\left(\lambda + cp_s T_s\right)\left(X_s - X_W\right)\sigma + h_{T,s}\left(T_s - T_W\right) + U_{T,p}\left(T_p - T_W\right) = 0 \tag{16}$$

$$\frac{d\dot{m}_w}{dy} = \frac{h_{M,s}\left(X_s - X_W\right)\sigma}{h/2} \tag{17}$$

The mass transfer coefficient h_M, assuming *Le=1* (Kim et al., 2015; Stabat and Marchio, 2004), has been calculated as:

$$h_M = \frac{h_T}{cp_a} \tag{18}$$

The heat transfer coefficient h_T was calculated using the following correlation (De Antonellis et al., 2017):

$$h_T = \frac{k_a}{2\,h} 0.0185\,\mathrm{Re}^{0.928}\,\mathrm{Pr}^{1/3} \tag{19}$$

According to the previous research (De Antonellis et al., 2017), the correlation to predict the wettability factor σ is:

$$\sigma = \dot{m}_w \frac{h}{2\,\delta_w v_w \rho_w} = \dot{m}_w\, C_w \tag{20}$$

Where:

$$C_w = \frac{k_1}{v_S^{N\,k_2} e^{k_3\,\dot{m}_{w,in,HE}}} \tag{21}$$

And:

$$\dot{m}_{w,in,HE} = \dot{m}_{w,in} - \frac{\left(X_{s,in,HE} - X_{s,in}\right)\dot{Q}_S^N\ \rho^N}{3600\ A_{HE,net}} \tag{22}$$

$\dot{m}_{w,in,HE}$ is the water specific mass flow rate, net of the water evaporation in the secondary air inlet plenum, and

$$\dot{m}_{w,in} = \frac{\dot{M}_{w,in}}{A_{HE,net}} \tag{23}$$

The correlation to predict the saturation efficiency in the secondary air inlet plenum is (De Antonellis et al., 2017):

$$\varepsilon_h = \frac{c_1 \ln\left(T_{s,in} - T_{s,wb,in}\right) + c_2}{\dot{M}_s^{c_3}} \dot{M}_{w,in}^{c_4} \tag{24}$$

As discussed in section 2.3, the experimental setup, more precisely the air plenums, has been slightly modified compared to the previous research work (De Antonellis et al., 2017). Therefore, 30 experimental tests have been carried out (N_1 to N_6 in Table 3), in order to fit the wettability factor and saturation efficiency parameters reported in Eq. 21 and Eq. 24 (Liberati et al., 2017). Tests have been performed adopting the same methodology previously adopted (De Antonellis et al., 2017) and resulting coefficients are summarized in Table 5 (Liberati et al., 2017).

Table 5. Correlation coefficients for the detailed model (DM) of Eqs. 21 and 24 (Liberati et al., 2017).

Coefficient	Value
k_1	4.82
k_2	0.0114
k_3	4.8192
c_1	6.781
c_2	33.977
c_3	0.9547
c_4	0.9839

As shown in Fig. 4, there is a very good agreement between numerical and experimental primary air temperature variation, being the deviation always within 0.3 °C.

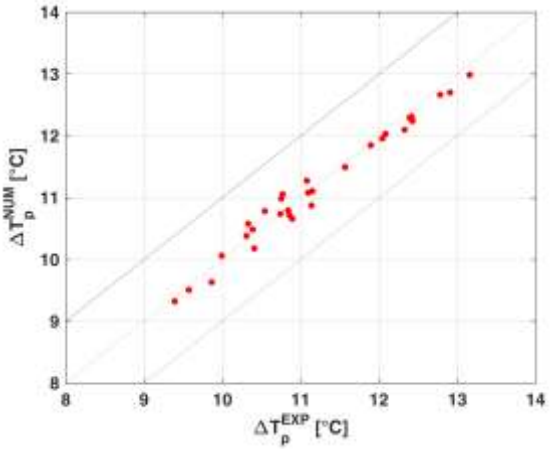

Fig. 4. Parity plot of experimental and numerical ΔT_p of the detailed model (tests N_1 - N_6 reported in Table 3).

4. Validation of the models: results and analysis

4.1 Preliminary comparison between detailed and simplified models

The results of the detailed and simplified models of the IEC system have been preliminary analysed by varying $T_{p,in}$, $T_{s,in}$, $X_{s,in}$, v_s^N and $\dot{Q}_{w,in}$, as shown in Fig. 5. In the analysis, the average value of each input variable adopted in the detailed model calibration has been used as reference condition. It can be observed the two models perform similarly: in the investigated range, also outputs of the detailed model, which is based on a phenomenological approach, show an almost linear response. In case of variation of $\dot{Q}_{w,in}$, although outputs response is not fully linear (as shown also by experimental results of Fig. 2), the deviation between the two models is very limited. Therefore, the first-order approach adopted in the simplified model can be assumed satisfactory to estimate the behaviour of the IEC system.

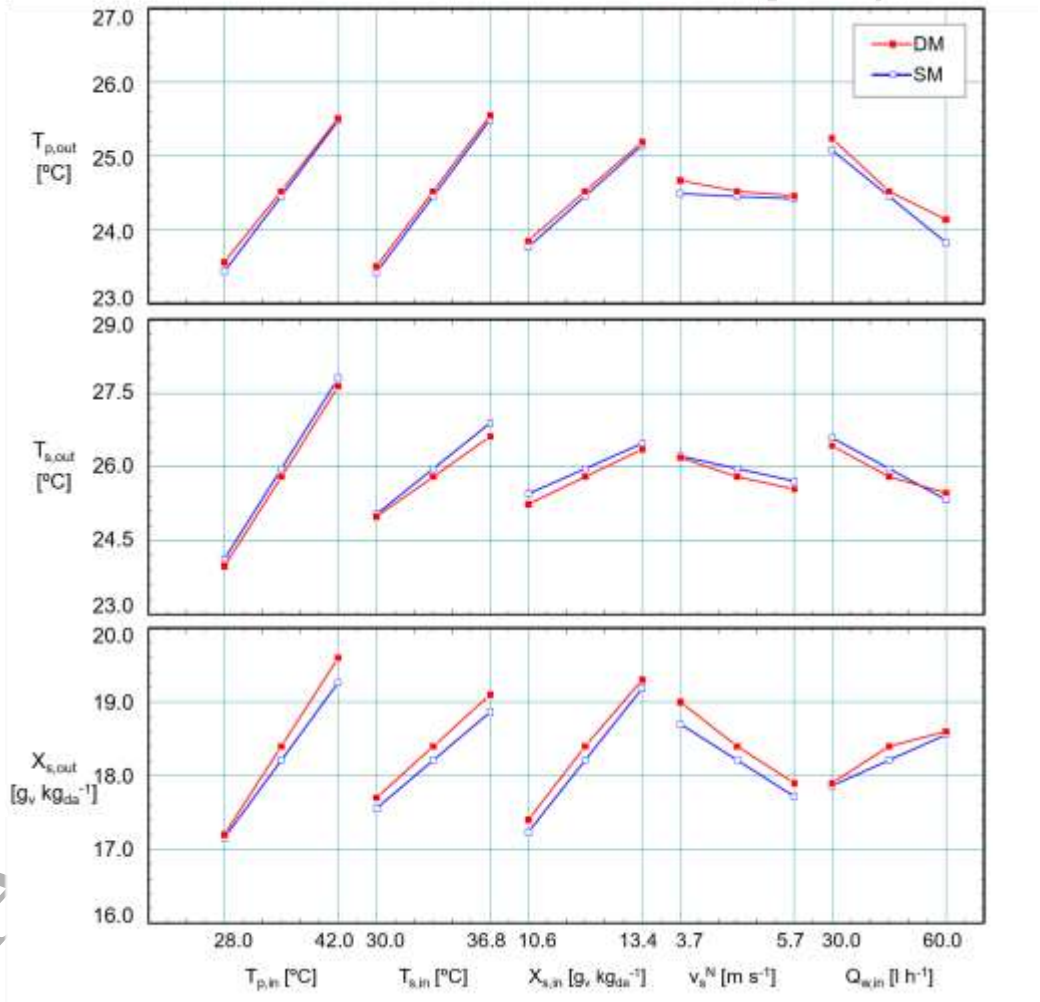

Fig. 5. Effect of inlet conditions on outputs of the simplified and detailed models. Reference inlet conditions: $T_{p,in}$=35.0 °C, $T_{s,in}$=33.4, $X_{s,in}$=12.0 g_v kg_{da}^{-1}, v_s^N = 4.7 m s^{-1}, v_p^N = 3.7 m s^{-1} and $\dot{Q}_{w,in}$= 45 l h^{-1}.

4.2 Description of case studies

Three case studies have been analysed in order to validate the models: experimental tests have been performed (tests N_{24} - N_{26} of Table 3) and compared to outputs of the models. The first case study is related to a data center application, the second one to a desiccant evaporative cooling (DEC) configuration and the third one to a residential application. In each case, the water flow rate $\dot{Q}_{w,in}$ has been varied between 30 and 65 l h^{-1}, while the remaining inputs have been set in this way:

- Case A (Data center application, test N_{24} of Table 3): the primary air stream is at data center ambient conditions ($T_{p,in}$ =35 °C) while the secondary air stream is at summer outdoor conditions ($T_{s,in}$ =30°C, $RH_{s,in}$=50%). This condition is similar to test N_1 and N_2 with a different secondary air flow rate.
- Case B (DEC configuration, test N_{25} of Table 3): the primary air stream is at outlet desiccant wheel conditions ($T_{p,in}$ =60 °C) while the secondary air stream is at indoor conditions (return air from the building $T_{s,in}$ =26°C, $RH_{s,in}$=60%).
- Case C (Residential configuration, test N_{26} of Table 3): the primary air stream is at outdoor conditions ($T_{p,in}$ =30 °C) while the secondary air stream is at indoor conditions (return air from the building $T_{s,in}$ =26°C, $RH_{s,in}$=60%).

The deviation between experimental data and calculated outputs has been evaluated by the Root Mean Standard Deviations, RMSD, and the percentage of the maximum deviation, MD. RMSD of the generic output Y (ΔT_p, ΔT_s, ΔX_s or ε_{wb}) has been calculated with Eq. 25, where N_T is the number of adopted tests in each case study.

$$RMSD_Y = \sqrt{\frac{\sum_{i=1}^{N}\left(Y^{NUM} - Y^{EXP}\right)^2}{N_T}} \tag{25}$$

4.3 Analysis of the case studies

As discussed in section 4.2, additional experimental tests were carried out in order to analyse the IEC behaviour under three different input air conditions and validate the two mathematical models. The obtained values of RMSD and of MD for the three case studies are reported in Table 6, while detailed experimental and numerical results are represented in Figs 6-8.

Table 6. RMSD values and MD for the three case studies.

Case study	ΔT_p				ΔT_s				ΔX_s				ε_{wb}			
	RMSD [ºC]		MD [%]		RMSD [ºC]		MD [%]		RMSD [$g_v\ kg_{da}^{-1}$]		MD [%]		RMSD [-]		MD [%]	
	DM	SM	DM	SM	DM	SM	DM	SM	DM	SM	DM	SM	DM	SM	DM	SM
A	0.18	0.29	0.85	1.66	0.34	0.39	1.56	1.76	0.18	0.13	1.21	0.90	0.01	0.02	1.85	3.40
B	0.38	0.74	2.36	3.43	0.56	0.83	2.98	4.08	0.62	0.42	4.02	3.13	0.01	0.02	2.05	2.96
C	0.12	0.06	0.68	0.47	0.26	0.33	1.69	1.80	0.24	0.25	1.92	1.85	0.01	0.01	1.93	1.33

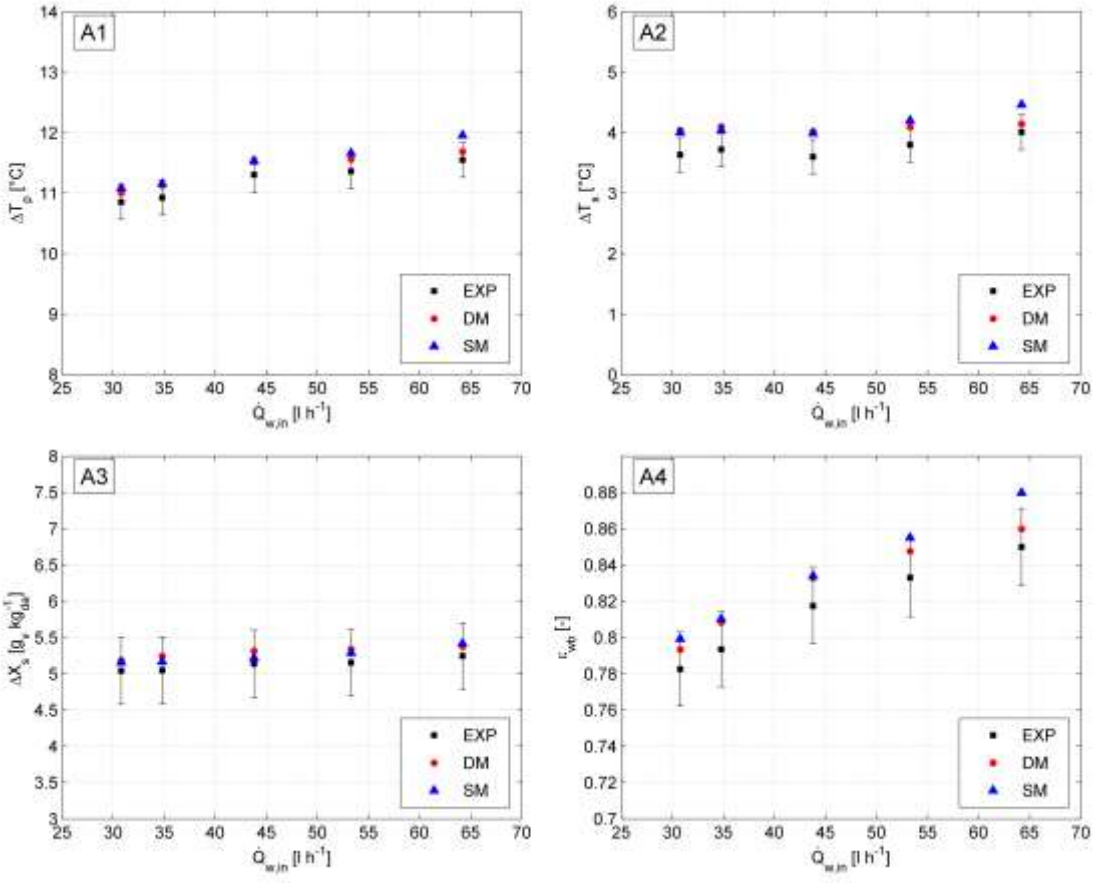

Fig. 6. Experimental and simulation results of ΔT_p, ΔT_s, ΔX_s and ε_{wb} as a function of $\dot{Q}_{w,in}$ for case study A.

It is highlighted that in all cases, the higher $\dot{Q}_{w,in}$, the higher ΔT_p, ΔT_s, ΔX_s and ε_{wb}. Previous studies showed similar trends in these four parameters when the water flow rate of IEC is varied (De Antonellis et al., 2016).

In Fig. 6, it is shown that numerical results of case A are in very good agreement with experimental data. The results of both models are always within or close to the experimental uncertainty of the measured data, except at high water flow rate for the simplified model. The maximum deviations of ε_{wb} is very small and equal to 1.85% and 3.40% respectively for DM and SM. Finally, the maximum values of ΔT_p, ΔT_s, ΔX_s and ε_{wb} obtained are 11.6 ºC, 4.0 ºC, 5.2 $g_v\ kg_{da}^{-1}$ and 0.85, respectively, while the minimum values are 10.9 ºC, 3.6 ºC, 5.0 $g_v\ kg_{da}^{-1}$ and 0.78.

Regarding case study B, the outputs trends reported in Fig. 7 are similar to those of case study A. However, negative values of ΔT_s occurred because the inlet primary air temperature was significantly hotter than the secondary air one. As a consequence, measured ΔT_p increased significantly, reaching 33.7 ºC at the maximum water flow rate, with a wet bulb effectiveness of 84%. Fig. 7 also highlights that the models correctly predict the behaviour of the IEC, although its operating conditions are far from the calibration range of the models. In this case study, the highest values of RMSD and MD of ΔT_p, ΔT_s and ε_{wb} have been calculated for the simplified model and of ΔX_s for the detailed model. Nevertheless, the values of MD are always below 5% for both models.

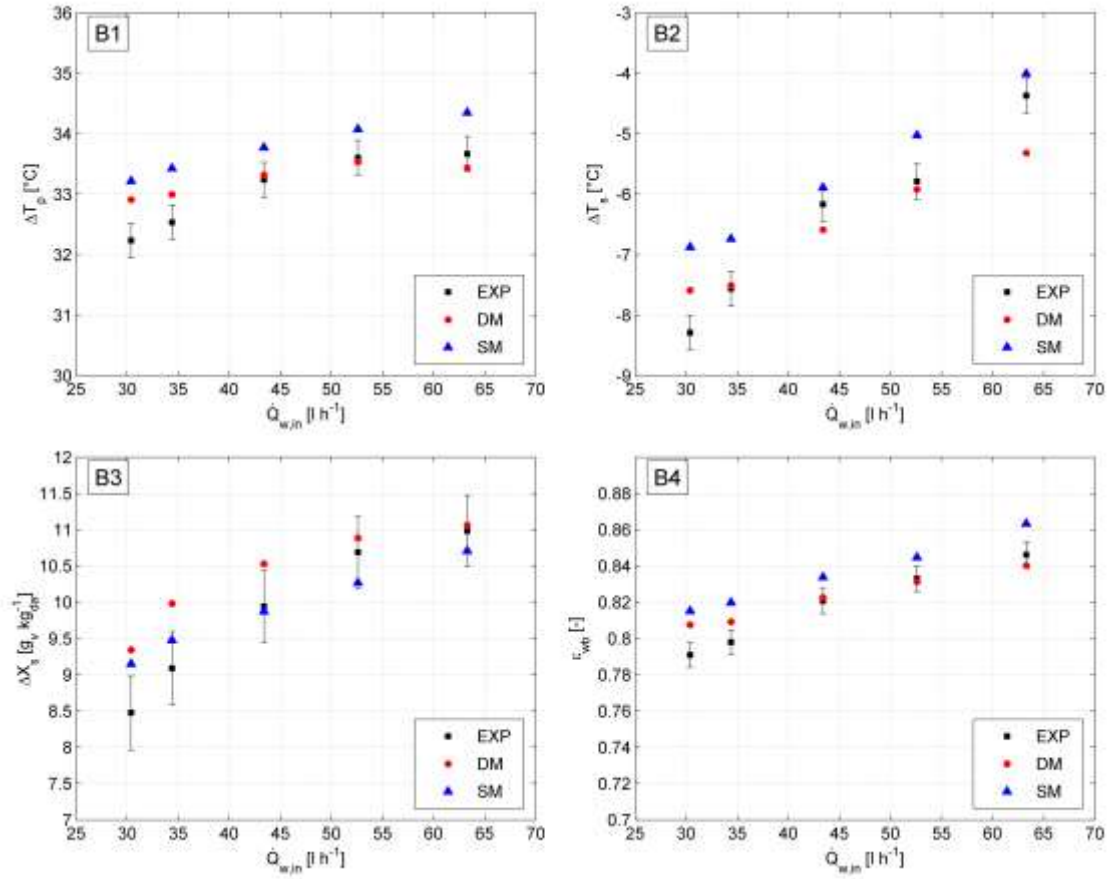

Fig. 7. Experimental and simulation results of ΔT_p, ΔT_s, ΔX_s and ε_{wb} as a function of $\dot{Q}_{w,in}$ for case study B.

Case study C has been carried out in typical residential conditions. Results show similar trends of case study A and B: the higher $\dot{Q}_{w,in}$, the higher the ΔT_p, ΔT_s, ΔX_s and ε_{wb}, as reported in Fig. 8. In additional, in this case study, the numerical results are in very good agreement with experimental data: the values of MD are always below 2% for the four parameters.

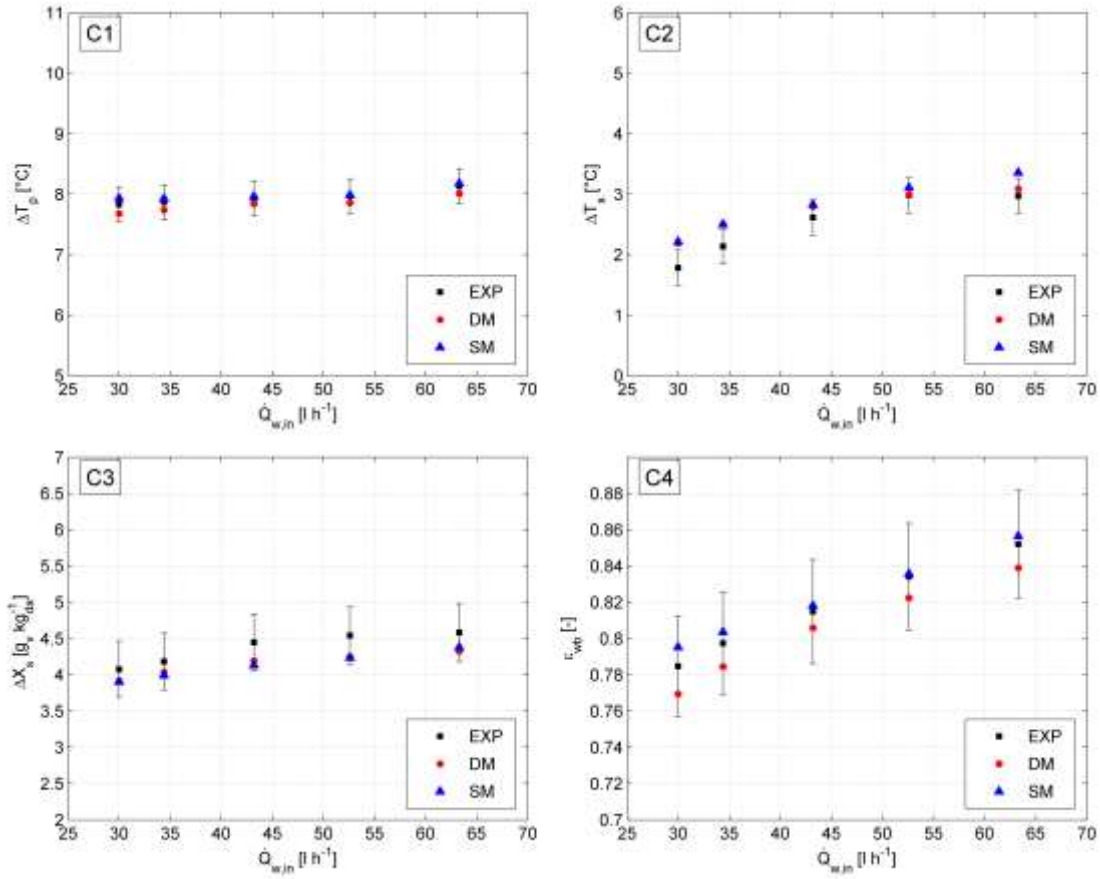

Fig. 8. Experimental and simulation results of ΔT_p, ΔT_s, ΔX_s and ε_{wb} as a function of $\dot{Q}_{w,in}$ for case study C.

4.4 Considerations about the use of the models

Based on the aforementioned results, it is possible to state that, in the investigated range of operating conditions, the simplified model performs similarly to the detailed one, despite its significantly lower computational load. For this reason, the empirical correlation (SM) based on the application of standard statistical technique should be preferred to the detailed approach (DM) for implementation in simulation tools. On the other side, the calibration process of the simplified model (for adaptation to different indirect evaporative coolers) is a critical issue, requiring several experimental data obtained in specific working conditions. If such information cannot be easily obtained from manufacturer data or through experimental tests, the empirical correlation could be calibrated through outputs of a detailed phenomenological model, as often carried out in the field (Jeong and Mumma, 2005).

Finally, it can be stated that the simplified model can be used to simulate:

– The IEC system described in section 2, in the following operating conditions (calibration range of Tab. 3): 25°C < $T_{s,in}$ < 38 °C, 8 g_v kg_{da}^{-1} < $X_{s,in}$ < 16 g_v kg_{da}^{-1}, 3.7 m s^{-1} < $v^N_{s,in}$ < 5.7 m s^{-1}, 28°C < $T_{p,in}$ < 48 °C and 30 l h^{-1} < $\dot{Q}_{w,in}$ < 60 l h^{-1}, with $v^N_{p,in}$ = 3.7

m s^{-1}. In section 4.3 it is also shown that the model properly predicts IEC system performance also outside the calibration range.

– A IEC system with a different number of plates (but with the same geometry and length). In this case, if $\dot{Q}''^{N}_{s,in}$, $\dot{Q}'_{w,in}$ and N'_{HE} are respectively the secondary air flow rate, the water flow rate and the number of plates of the IEC system, the simplified model inputs $v^{N}_{s,in}$ and $\dot{Q}_{w,in}$ are rearranged in this way:

$$v^{N}_{s,in} = \dot{Q}''^{N}_{s,in} / (3600\ (N'_{HE} - 1)\ h\ L^{*}/2\ ) \quad (26)$$

$$\dot{Q}_{w,in} = \dot{Q}'_{w,in}\ (N_{HE} - 1)/(N'_{HE} - 1) \quad (27)$$

Note that it is $v^{N}_{p,in}$ = const. = 3.7 m s^{-1} and, therefore, the primary air flow directly depends on the number of plates.

Therefore, the simplified mathematical model obtained is suitable for integration in simulation tools, being able to be combined with other HVAC elements, in order to study the global behaviour of hybrid systems. For instance, the model can be used to perform yearly energy analysis of an IEC coupled with a desiccant wheel or a conventional chiller.

5. Conclusions

In this work, a simplified IEC model, based on a first order linear regression approach, has been developed. This model can be used to predict the influence of $T_{p,in}$, $T_{s,in}$, $X_{s,in}$, v_p^{N} and $\dot{Q}_{w,in}$, on the output variables $T_{p,out}$, $T_{s,out}$ and $X_{s,out}$. The model effectively correlates experimental data: R^2 values, obtained considering all the 37 adopted tests, are 99.54 % for $T_{p,out}$, 99.78 % for $T_{s,out}$ and 99.89 % for $X_{s,out}$.

The simplified model (SM) has been compared with results of a detailed one (DM) and with further experimental data. Three cases studies have investigated in order to analyse the IEC system and compare the accuracy of both models. Each case study deals with typical air conditions of actual IEC applications. Numerical results of both models are in agreement with experimental data in all the case studies: the maximum deviations are obtained for the case study B, DEC configuration, whose inlet conditions are outside the calibration range of the two models. Nevertheless, deviations of wet bulb effectiveness are always below 2.05 % for the detailed model and 3.40 % for the simplified one.

Finally, it is possible to state that the simplified IEC model can be effectively integrated in energy simulation tools, due to its low computational load and good accuracy. Whereas, the detailed model is suitable to design and optimize indirect evaporative coolers, being more accurate than SM and based on a phenomenological approach.

Acknowledgements

The authors would like to acknowledge Mr Leone, Mr Bawa and Mr Liberati of Recuperator S.p.A. for their economical and technical support.

References

Agrawal, A., Khichar, M., Jain, S., 2016. Transient simulation of wet cooling strategies for a data center in worldwide climate zones. Energy Build. 127, 352–359. https://doi.org/10.1016/j.enbuild.2016.06.011

Chen, Y., Luo, Y., Yang, H., 2014. Fresh air pre-cooling and energy recovery by using indirect evaporative cooling in hot and humid region - A case study in Hong Kong. Energy Procedia 61, 126–130. https://doi.org/10.1016/j.egypro.2014.11.922

Chung, J.D., Lee, D.Y., 2011. Contributions of system components and operating conditions to the performance of desiccant cooling systems. Int. J. Refrig. 34, 922–927. https://doi.org/10.1016/j.ijrefrig.2011.03.003

Cui, X., Chua, K.J., Islam, M.R., Ng, K.C., 2015. Performance evaluation of an indirect pre-cooling evaporative heat exchanger operating in hot and humid climate. Energy Convers. Manag. 102, 140–150. https://doi.org/10.1016/j.enconman.2015.02.025

Cui, X., Chua, K.J., Yang, W.M., 2014. Numerical simulation of a novel energy-efficient dew-point evaporative air cooler. Appl. Energy 136, 979–988. https://doi.org/10.1016/j.apenergy.2014.04.040

De Antonellis, S., Joppolo, C.M., Liberati, P., Milani, S., Molinaroli, L., 2016. Experimental analysis of a cross flow indirect evaporative cooling system. Energy Build. 121, 130–138. https://doi.org/10.1016/j.enbuild.2016.03.076

De Antonellis, S., Joppolo, C.M., Liberati, P., Milani, S., Romano, F., 2017. Modeling and experimental study of an indirect evaporative cooler. Energy Build. 142, 147–157. https://doi.org/10.1016/j.enbuild.2017.02.057

DIN EN ISO 5167-2 Standards, 2003. Masurement of a fluid flow by means of pressure differential devices inserted in circular cross-section conduits running full - Part 2: Orifice plates (ISO 5167-2).

Duan, Z., Zhan, C., Zhang, X., Mustafa, M., Zhao, X., Alimohammadisagvand, B., Hasan, A., 2012. Indirect evaporative cooling: Past, present and future potentials. Renew. Sustain. Energy Rev. 16, 6823–6850. https://doi.org/10.1016/j.rser.2012.07.007

Elgendy, E., Mostafa, A., Fatouh, M., 2015. Performance enhancement of a desiccant evaporative cooling system using direct/indirect evaporative cooler. Int. J. Refrig. 51, 77–

87. https://doi.org/10.1016/j.ijrefrig.2014.12.009

Erens, P.J., Dreyer, A.A., 1993. Modelling of indirect evaporative air coolers. Int. J. Heat Mass Transf. 36, 17–26. https://doi.org/10.1016/0017-9310(93)80062-Y

Goldsworthy, M., White, S., 2011. Optimisation of a desiccant cooling system design with indirect evaporative cooler. Int. J. Refrig. 34, 148–158. https://doi.org/10.1016/j.ijrefrig.2010.07.005

Gómez, E.V., Martínez, F.J.R., Diez, F.V., Leyva, M.J.M., Martín, R.H., 2005. Description and experimental results of a semi-indirect ceramic evaporative cooler. Int. J. Refrig. 28, 654–662. https://doi.org/10.1016/j.ijrefrig.2005.01.004

González Cruz, E., Krüger, E., 2015. Evaluating the potential of an indirect evaporative passive cooling system for Brazilian dwellings. Build. Environ. 87, 265–273. https://doi.org/10.1016/j.buildenv.2015.01.020

Guo, X.C., Zhao, T.S., 1998. A parametric study of an indirect evaporative air cooler. Int. Commun. Heat Mass Transf. 25, 217–226. https://doi.org/10.1016/S0735-1933(98)00008-6

Hasan, A., 2012. Going below the wet-bulb temperature by indirect evaporative cooling: Analysis using a modified ε-NTU method. Appl. Energy 89, 237–245. https://doi.org/10.1016/j.apenergy.2011.07.005

Heidarinejad, G., Bozorgmehr, M., Delfani, S., Esmaeelian, J., 2009. Experimental investigation of two-stage indirect/direct evaporative cooling system in various climatic conditions. Build. Environ. 44, 2073–2079. https://doi.org/10.1016/j.buildenv.2009.02.017

Hettiarachchi, H.D.M., Golubovic, M., Worek, W.M., 2007. The effect of longitudinal heat conduction in cross flow indirect evaporative air coolers. Appl. Therm. Eng. 27, 1841–1848. https://doi.org/10.1016/j.applthermaleng.2007.01.014

ISO, 2008. Evaluation of measurement data — Guide to the expression of uncertainty in measurement. Int. Organ. Stand. Geneva ISBN 50, 134. https://doi.org/10.1373/clinchem.2003.030528

Jeong, J.W., Mumma, S.A., 2005. Practical thermal performance correlations for molecular sieve and silica gel loaded enthalpy wheels. Appl. Therm. Eng. 25, 719–740. https://doi.org/10.1016/j.applthermaleng.2004.07.018

Kim, M.H., Jeong, D.S., Jeong, J.W., 2015. Practical thermal performance correlations for a wet-coil indirect evaporative cooler. Energy Build. 96, 285–298. https://doi.org/10.1016/j.enbuild.2015.03.043

Kim, M.H., Kim, J.H., Choi, A.S., Jeong, J.W., 2011. Experimental study on the heat exchange effectiveness of a dry coil indirect evaporation cooler under various operating conditions. Energy 36, 6479–6489. https://doi.org/10.1016/j.energy.2011.09.018

Liberati, P., De Antonellis, S., Leone, C., Joppolo, C.M., Bawa, Y., 2017. Indirect evaporative cooling systems: modelling and performance analysis. Energy Procedia 140, 475–485. https://doi.org/10.1016/j.egypro.2017.11.159

Maclaine-cross, I.L., Banks, P.J., 1981. A General Theory of Wet Surface Heat Exchangers and its Application to Regenerative Evaporative Cooling. J. Heat Transfer 103, 579–585.

Merkel, F., 1925. Verdunstungskühlung. VDI-Zeitchrift 123–8.

Moffat, R.J., 1988. Describing the uncertainties in experimental results. Exp. Therm. Fluid Sci. 1, 3–17. https://doi.org/10.1016/0894-1777(88)90043-X

Montgomery, D.C., 2004. Design and analysis of experiments, 6th Edition. Wiley.

Pandelidis, D., Anisimov, S., 2016. Application of a statistical design for analyzing basic performance characteristics of the cross-flow Maisotsenko cycle heat exchanger. Int. J. Heat Mass Transf. 95, 45–61. https://doi.org/10.1016/j.ijheatmasstransfer.2015.11.060

Pandelidis, D., Anisimov, S., Worek, W.M., Drag, P., 2016. Comparison of desiccant air conditioning systems with different indirect evaporative air coolers. Energy Convers. Manag. 117, 375–392. https://doi.org/10.1016/j.enconman.2016.02.085

Poppe, M., Rögener, H., 1984. Evaporative cooling systems. VDI-Warmeatlas, Sect. Mh.

Ren, C., Yang, H., 2006. An analytical model for the heat and mass transfer processes in indirect evaporative cooling with parallel/counter flow configurations. Int. J. Heat Mass Transf. 49, 617–627. https://doi.org/10.1016/j.ijheatmasstransfer.2005.08.019

Sohani, A., Sayyaadi, H., Hoseinpoori, S., 2016. Modeling and multi-objective optimization of an M-cycle cross-flow indirect evaporative cooler using the GMDH type neural network. Int. J. Refrig. 69, 186–204. https://doi.org/10.1016/j.ijrefrig.2016.05.011

Stabat, P., Marchio, D., 2004. Simplified model for indirect-contact evaporative cooling-tower behaviour. Appl. Energy 78, 433–451. https://doi.org/10.1016/j.apenergy.2003.09.004

Statgraphics Centurion XV , 2006. (http://www.statgraphics.com/) (accessed 08.02.18)

Tejero-González, A., Andrés-Chicote, M., Velasco-Gómez, E., Rey-Martínez, F.J., 2013. Influence of constructive parameters on the performance of two indirect evaporative cooler prototypes. Appl. Therm. Eng. 51, 1017–1025. https://doi.org/10.1016/j.applthermaleng.2012.10.054

Velasco Gómez, E., Tejero González, A., Rey Martínez, F.J., 2012. Experimental characterisation of an indirect evaporative cooling prototype in two operating modes. Appl. Energy 97, 340–346. https://doi.org/10.1016/j.apenergy.2011.12.065